

# Time-resolved laser-induced incandescence from multiwalled carbon nanotubes in air

J. M. Mitrani<sup>1,a)</sup> and M. N. Shneider<sup>2</sup>

<sup>1</sup>Princeton Plasma Physics Laboratory, Princeton, New Jersey 08540, USA

<sup>2</sup>Department of Mechanical Engineering, Princeton University, Princeton, New Jersey 08544, USA

(Received 2 December 2014; accepted 19 January 2015; published online 28 January 2015)

We observed temporal laser-induced incandescence (LII) signals from multiwalled carbon nanotubes (MWCNTs) suspended in ambient air. Unlike previous LII experiments with soot particles, which showed that primary particles with larger diameters cool at slower timescales relative to smaller particles, we observed that thicker MWCNTs with larger outer diameters (ODs) cool at faster timescales relative to thinner MWCNTs with smaller ODs. We suggested a simple explanation of this effect, based on the solution of one-dimensional nonstationary heat conduction equation for the initial non-uniform heating of MWCNTs with ODs greater than the skin depth.

© 2015 AIP Publishing LLC. [<http://dx.doi.org/10.1063/1.4907000>]

Laser-induced incandescence (LII) is a powerful diagnostic used for *in situ* monitoring of nanoparticles and has been extensively used as a combustion and pollution diagnostic to monitor soot particles in background flames.<sup>1–4</sup> A time-resolved LII diagnostic involves heating nanoparticles with a short-pulsed laser, and recording the time evolution of the induced incandescence signals. For soot particles, since laser energy absorption is proportional to volume, and cooling through heat conduction to the ambient gas is proportional to surface area, LII signals from larger soot particles will have longer incandescence times than LII signals from smaller particles, enabling LII to be used as an *in situ* sizing diagnostic.

Recently, LII has been applied to monitor volumetric synthesis of nanoparticles by the flame spray pyrolysis<sup>5</sup> and microwave plasma discharge<sup>6</sup> methods. More understanding of the heat transfer processes involved with volumetric laser heating of nanoparticles needed in order for LII to be used as an *in situ* sizing diagnostic for engineered carbon nanoparticles.<sup>7</sup> Specifically, unlike soot particles, carbon nanotubes (CNTs) are hollow and cylindrical, so different heat transfer processes may dominate laser energy absorption and cooling for CNTs. It is essential to have an accurate understanding of the relevant heat transfer processes in order for LII to be applied as a diagnostic to monitor volumetric synthesis of CNTs, and other nanoparticles.

We have therefore constructed a setup (Figure 1), which allows for observation of LII on research-grade, commercially available multiwalled CNTs (MWCNTs), with known sizes and structures. The two types of MWCNTs chosen for this study were manufactured under similar conditions (Reade) and had lengths of around 1  $\mu\text{m}$ , but had different outer diameters (ODs) and inner diameters (IDs), which enabled us to observe the effects of MWCNT thickness on temporal LII signals. “Thicker” MWCNTs had ODs and IDs of 30 nm and 8 nm, respectively. “Thinner” MWCNTs had ODs and IDs of 12 nm and 4 nm, respectively. We built a

device that suspended MWCNT powders in air with a piezoelectric disk (Piezo Systems). This device is previously described elsewhere,<sup>8</sup> with additional modifications for this application. The suspended nanoparticles were heated with a laser beam sheet, generated from a 1064 nm, Q-switched Nd:YAG laser (Quantel 100 Stable). To control the beam sheet fluence ( $\text{J}/\text{cm}^2$ ), we modulated the beam energy with a half-wave plate and polarizer (Thorlabs), and measured the beam sheet energy and area with an energy meter (Coherent Fieldmax II) and a beam profiler (Ophir Spiricon SP620U), respectively. Temporal LII signals (Figure 2) from thicker MWCNTs with larger ODs and thinner MWCNTs with smaller ODs were collected with achromatic lenses, narrow bandpass filters with center wavelengths of  $\lambda_{\text{CWL}} = 550$  and 420 nm, and two photomultiplier tubes (Hamamatsu H10721–20, and R1463).

Our observed temporal LII signals from thicker MWCNTs (red squares) have a faster incandescence times than LII signals from thinner MWCNTs (green diamonds). This effect is more easily seen at a fluence of 0.1  $\text{J}/\text{cm}^2$

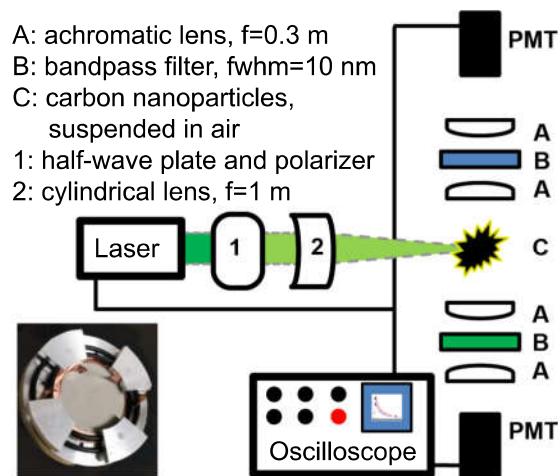


FIG. 1. Top-down schematic of experimental setup. Inset: piezoelectric disk mounted in a device, which we used to suspend nanoparticles.

<sup>a)</sup>Electronic mail: [jmitrani@pppl.gov](mailto:jmitrani@pppl.gov)

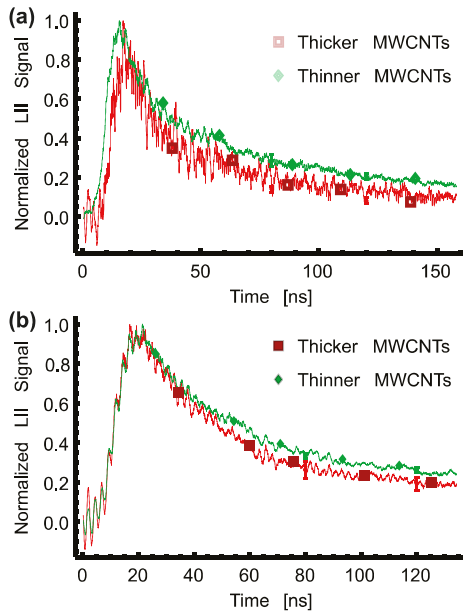


FIG. 2. Temporal LII signals, normalized to their peak intensity, from MWCNTs. The signals were recorded with laser fluences of (a)  $0.1 \text{ J/cm}^2$  and (b)  $0.2 \text{ J/cm}^2$ . Red squares and green diamonds represent thicker and thinner MWCNTs, with ODs of 30 nm and 12 nm, respectively. Temporal LII signals from thicker MWCNTs have faster incandescence times than temporal LII signals from thinner MWCNTs, an effect more easily observed at lower laser fluences.

(Figure 2). The reason that LII signals from thicker MWCNTs have relatively faster incandescence times is due to differences in the heat transfer profiles of the thicker and thinner MWCNTs.

A simple, qualitative explanation of this effect involves studying the relevant heat transfer profiles for the MWCNTs in our experiment. We used the solution of the 1D nonstationary heat conduction equation

$$\frac{\partial T}{\partial t} = \chi \frac{1}{r} \frac{\partial}{\partial r} \left( r \frac{\partial T}{\partial r} \right), \quad (1)$$

where  $\chi = \kappa / (\rho c_p) \sim 10^{-3} \text{ cm}^2/\text{s}$ ,  $\kappa \sim 0.005 \text{ W/cm} \cdot \text{K}$ ,<sup>9</sup>  $\rho \sim 2.1 \text{ g/cm}^3$ , and  $c_p \sim 2 \text{ J/g} \cdot \text{K}$ , are the thermal diffusivity, transverse thermal conductivity, mass density, and specific heat capacity, respectively, to model the radial temperature distribution for MWCNTs, initially ( $< 10 \text{ ns}$ ) after laser heating (Figure 3). For simplicity,  $\kappa$  was assumed to be constant in the radial direction. The skin depth for laser heated MWCNTs is

$$\delta = (0.5\sigma\omega\mu)^{-1/2} \approx 13.4 \text{ nm}, \quad (2)$$

where  $\sigma \sim 5 \times 10^4 \text{ S/cm}$ ,<sup>10</sup>  $\omega = 2\pi c/\lambda_L$ ,  $\lambda_L = 1064 \text{ nm}$ ,  $\mu \sim \mu_0$ , are the electrical conductivity, angular laser frequency, laser wavelength, and permeability, respectively. Since  $OD_{Thin} \ll \delta < OD_{Thick}$ , the thinner and thicker MWCNTs have different initial, radial temperature profiles,  $T(r, t=0)$ , resulting in different heat transfer processes dominating the respective cooling rates. The cooling times for the MWCNTs due to radial thermal diffusion,  $\tau_{Diff}$ , and conduction to the ambient gas,  $\tau_{Cond}$ , are

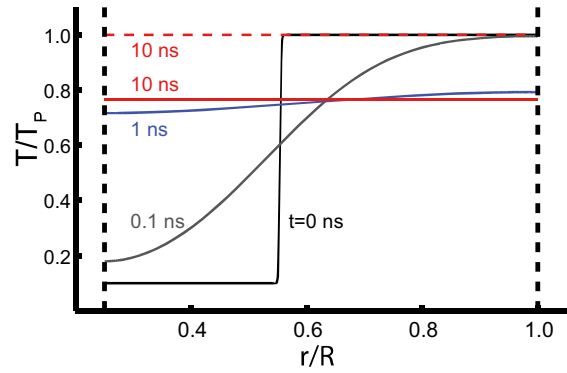


FIG. 3. Qualitative description of temporal temperature distribution,  $T(r, t)$ , for thicker (solid) and thinner (dashed) MWCNTs.  $T_p$  and  $R$  refer to the peak temperature and OD for the thinner and thicker MWCNTs. For the thicker MWCNTs,  $T(r, t)$  is shown at different times after the laser pulse. For  $t = 10 \text{ ns}$  after the laser pulse, the thicker and thinner MWCNTs both have uniform radial temperature profiles, but the temperature is lower for the thicker MWCNTs (solid) than for the thinner MWCNTs (dashed).

$$\tau_{Diff} = R^2/\chi \approx 8 \text{ ns}, \quad (3a)$$

$$\tau_{Cond} \sim R/(\xi/\rho c_p) \approx 3 \mu\text{s}, \quad (3b)$$

where  $R$  is the characteristic radius, and  $\xi \sim 4 \text{ W/cm}^2 \cdot \text{K}$ , is a coefficient for heat conduction to the ambient gas. A standard LII term for heat conduction per unit area,  $Q_{Cond}$ , is used to derive  $\xi$ , where<sup>11</sup>

$$Q_{Cond} = \xi \cdot \Delta T = \frac{\alpha_T P_0}{2T_0} \left( \frac{\gamma + 1}{\gamma - 1} \right) \sqrt{\frac{R_M T_0}{2\pi W_A}} \cdot \Delta T, \quad (4)$$

and  $\alpha_T$ ,  $P_0$ ,  $T_0$ ,  $R_M$ ,  $W_A$ , and  $\Delta T$  are the thermal accommodation coefficient, gas pressure, gas temperature, ideal gas constant (in units of  $\text{g cm}^2/\text{mol K s}^2$ ), molecular weight of air, and the difference in temperatures between the MWCNTs and air, respectively. Boundary conditions used for the heat conduction equation (Eq. (1)) were  $\frac{\partial T}{\partial r}|_{r=ID} = 0$  and  $-\kappa \frac{\partial T}{\partial r}|_{r=OD} = \xi \Delta T$ , where for simplicity, heat conduction along the inner wall of the MWCNT was assumed negligible.

Figure 4 shows a schematic that summarizes the differences in heat transfer profiles between the thinner and thicker MWCNTs. Because the thicker MWCNTs experience non-uniform radial heating, the heat transfer profiles of the thicker MWCNTs are significantly influenced by radial diffusion, which is a much faster cooling process than thermal conduction to the ambient gas (Eq. (3)), and which results in the thicker MWCNTs cooling at faster timescales than the thinner MWCNTs. This results in our observed temporal LII signals from the thicker MWCNTs decaying more quickly than the LII signals from the thinner MWCNTs.

Our simple, qualitative model does not include numerous endothermic and exothermic processes that may or may not influence the heat transfer profiles of the MWCNTs in our experiment. Relevant endothermic processes include: radiation, sublimation, photodesorption,<sup>12</sup> unzipping of MWCNTs,<sup>13</sup> exfoliation of single layer and few layer graphene flakes,<sup>14,15</sup> and formation of defects, such as Stone-Wales defects<sup>16</sup> and other large ring defects.<sup>17</sup> At atmospheric pressures, particle cooling by blackbody radiation is negligible with respect to

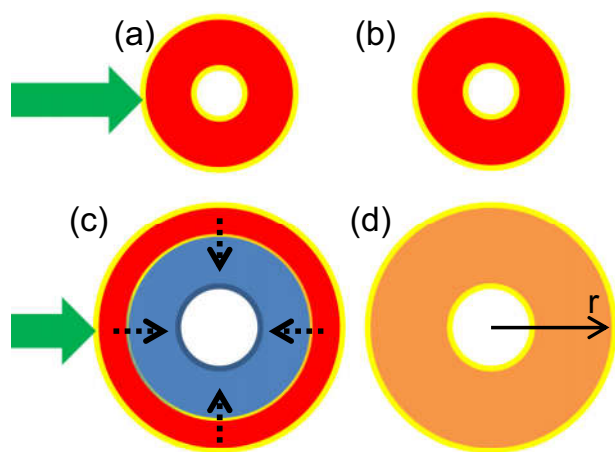


FIG. 4. Schematic showing radial cross-section of heat transfer profiles for thinner (top) and thicker (bottom) MWCNTs. (a) Since thinner MWCNTs have ODs comparable to the skin depth,  $\delta$ , laser heating (green, thick arrow) results in a uniform radial temperature profile. (b) After laser heating, thinner MWCNTs cool by thermal conduction to the ambient gas. (c) Since thicker MWCNTs have ODs greater than the skin depth,  $\delta$ , laser heating results in a non-uniform radial temperature profile. Thermal diffusion (black, dashed arrows) occurs initially after laser heating. (d) Thermal diffusion rapidly results in the thicker MWCNTs having a uniform radial temperature profile at a lower temperature. Because the timescales for diffusion are extremely short relative to thermal conduction, the thicker MWCNTs reach a lower temperature faster than the thinner MWCNTs.

thermal conduction. Relevant exothermic processes include annealing and oxidation.<sup>12</sup> Previous LII studies suggest that laser fluences higher than  $0.2\text{--}0.3\text{ J/cm}^2$  induce sublimation in soot particles, where small carbon clusters (primarily C, C<sub>2</sub>, and C<sub>3</sub>) are rapidly ejected from the particle surface.<sup>1,12</sup> For CNTs, high laser intensities may induce the formation of Stone-Wales defects, where a pair of pentagonal and heptagonal carbon rings are formed in place of the standard hexagonal rings found in graphite and CNTs. The formation of Stone-Wales defects structurally weakens the CNTs and results in a rapid release of energy.<sup>18–20</sup> However, previous experimental studies have suggested that heat treatment of MWCNTs by ovens<sup>21</sup> and CW lasers<sup>22</sup> may result in annealing, or the removal of defects from MWCNTs. Additionally, the presence of O<sub>2</sub> in air can cause oxidation reactions, resulting in the production of CO and CO<sub>2</sub> in the presence of carbon particles (e.g., CNTs, soot, and carbon black). Both annealing and oxidation are exothermic processes, which increase the internal temperature of the particle. Note that photodesorption and oxidation are more prominent for LII studies using UV lasers with higher energy photons.<sup>23</sup> Additionally, these aforementioned heat transfer processes are all more prominent at higher laser fluences, which may explain why one of our results—thicker MWCNTs cool more quickly than thinner MWCNTs—is more easily observed at lower laser fluences (Figure 2). This is consistent with the trend in previous LII studies, which recommends using lower laser fluences ( $<0.2\text{--}0.3\text{ J/cm}^2$ ) when applying LII as a diagnostic for sizing soot particles in flames.<sup>24,25</sup>

We presented observations of time-resolved LII signals from a high purity, MWCNT powder, as well as the observations of volumetric laser heating of MWCNTs. We observed that temporal LII signals from thicker MWCNTs have faster

decay times than LII signals from thinner MWCNTs. This is strikingly different from previous LII studies of soot particles with various sizes, where LII signals from soot particles with larger diameters have slower incandescence times than LII signals from soot particles with smaller diameters.<sup>4</sup> We proposed a simple, qualitative explanation for why, unlike soot, LII signals from thicker MWCNTs have faster incandescence times than LII signals from thinner MWCNTs. The thicker MWCNTs with ODs greater than the skin depth initially experience inhomogeneous laser heating, so the cooling time is dominated by thermal diffusion across the MWCNT. In contrast, since the thinner MWCNTs experience homogeneous laser heating, thermal diffusion across the MWCNT is negligible, and the cooling time is dominated by heat conduction to the ambient gas, which is a slower process than thermal diffusion. The solution of the 1D heat equation (Figure 3) confirms that the thicker MWCNTs cool at faster timescales than the thinner MWCNTs initially after laser heating.

By utilizing a setup designed to measure LII signals from research-grade nanoparticles with known sizes and structures, we can comprehensively study the heat transfer processes behind laser heated carbon nanoparticles, such as MWCNTs, SWCNTs, C<sub>60</sub>, and graphene flakes. As stated previously, a self-consistent, thorough model of LII in CNTs needs to incorporate various heat transfer processes, such as sublimation, defect formation, annealing, and oxidation. More research is needed in accurately quantifying the magnitudes and timescales of these heat transfer processes in the presence of different experimental conditions, including but not limited to: particle type (CNT, soot, and carbon black), initial particle temperature, background gas type and pressure, laser fluence ( $\text{J/cm}^2$ ), laser wavelength (or photon energy), and pulse duration. In addition to studying the effect of these heat transfer processes on our observed LII signals, we will analyze LII signals from our setup in order to calibrate LII as a diagnostic for *in situ* monitoring of volumetric synthesis of carbon nanoparticles at atmospheric pressures, and to further study heat transfer processes behind the volumetric synthesis of carbon nanoparticles.

The authors thank Y. Raites, B. C. Stratton, S. Patel, and A. Merzhvskiy for assistance. This work was supported by the U.S. Department of Energy, Office of Science, Basic Energy Sciences, Materials Sciences and Engineering Division. James M. Mitrani acknowledges support through the Program Plasma Science and Technology, at Princeton Plasma Physics Laboratory.

<sup>1</sup>C. Schulz, B. F. Kock, M. Hofmann, H. Michelsen, S. Will, B. Bougie, R. Suintz, and G. Smallwood, *Appl. Phys. B* **83**, 333 (2006).

<sup>2</sup>H. Bladh, J. Johnsson, J. Rissler, H. Abdulhamid, N.-E. Olofsson, M. Sanati, J. Pagels, and P.-E. Bengtsson, *Appl. Phys. B* **104**, 331 (2011).

<sup>3</sup>K. A. Thomson, D. R. Snelling, G. J. Smallwood, and F. Liu, *Appl. Phys. B* **83**, 469 (2006).

<sup>4</sup>R. L. V. Wal, T. M. Ticich, and A. B. Stephens, *Combust. Flame* **116**, 291 (1999).

<sup>5</sup>R. L. V. Wal, G. M. Berger, T. M. Ticich, and P. D. Patel, *Appl. Opt.* **41**, 5678 (2002).

<sup>6</sup>T. Sipkens, R. Mansmann, K. Daun, N. Petermann, J. Titantah, M. Karttunen, H. Wiggers, T. Dreier, and C. Schulz, *Appl. Phys. B* **116**, 623 (2013).

- <sup>7</sup>D. E. Rosner, *Ind. Eng. Chem. Res.* **44**, 6045 (2005).
- <sup>8</sup>A. Roquemore, B. John, F. Friesen, K. Hartzfeld, and D. Mansfield, *Fusion Eng. Des.* **86**, 1355 (2011).
- <sup>9</sup>J. G. Park, Q. Cheng, J. Lu, J. Bao, S. Li, Y. Tian, Z. Liang, C. Zhang, and B. Wang, *Carbon* **50**, 2083 (2012).
- <sup>10</sup>B. Marinho, M. Ghislandi, E. Tkalya, C. E. Koning, and G. de With, *Powder Technol.* **221**, 351 (2012).
- <sup>11</sup>H. Michelsen, F. Liu, B. F. Kock, H. Bladh, A. Boiariuc, M. Charwath, T. Dreier, R. Hadeif, M. Hofmann, J. Reimann, S. Will, P. Bengtsson, H. Bockhorn, F. Foucher, K. Geigle, C. Mounaim-Rousselle, C. Schulz, R. Stim, B. Tribalet, and R. Suntz, *Appl. Phys. B* **87**, 503 (2007).
- <sup>12</sup>H. A. Michelsen, *J. Chem. Phys.* **118**, 7012 (2003).
- <sup>13</sup>P. Kumar, L. Panchakarla, and C. Rao, *Nanoscale* **3**, 2127 (2011).
- <sup>14</sup>P. Kumar, *RSC Adv.* **3**, 11987 (2013).
- <sup>15</sup>U. Maitra, H. Matte, P. Kumar, and C. Rao, *CHIMIA Int. J. Chem.* **66**, 941 (2012).
- <sup>16</sup>A. Stone and D. Wales, *Chem. Phys. Lett.* **128**, 501 (1986).
- <sup>17</sup>S. L. Mielke, D. Troya, S. Zhang, J.-L. Li, S. Xiao, R. Car, R. S. Ruoff, G. C. Schatz, and T. Belytschko, *Chem. Phys. Lett.* **390**, 413 (2004).
- <sup>18</sup>K. Suenaga, H. Wakabayashi, M. Koshino, Y. Sato, K. Urita, and S. Iijima, *Nat. Nanotechnol.* **2**, 358 (2007).
- <sup>19</sup>L. Zhou and S.-Q. Shi, *Appl. Phys. Lett.* **83**, 1222 (2003).
- <sup>20</sup>M. B. Nardelli, B. Yakobson, and J. Bernholc, *Phys. Rev. Lett.* **81**, 4656 (1998).
- <sup>21</sup>Y. Kim, T. Hayashi, K. Osawa, M. Dresselhaus, and M. Endo, *Chem. Phys. Lett.* **380**, 319 (2003).
- <sup>22</sup>Z. H. Lim, A. Lee, K. Y. Y. Lim, Y. Zhu, and C.-H. Sow, *J. Appl. Phys.* **107**, 064319 (2010).
- <sup>23</sup>T. Savage, S. Bhattacharya, B. Sadanadan, J. Gaillard, T. Tritt, Y. Sun, Y. Wu, S. Nayak, R. Car, N. Marzari *et al.*, *J. Phys.: Condens. Matter* **15**, 5915 (2003).
- <sup>24</sup>F. Liu, M. Yang, F. A. Hill, D. R. Snelling, and G. J. Smallwood, *Appl. Phys. B* **83**, 383 (2006).
- <sup>25</sup>D. R. Snelling, F. Liu, G. J. Smallwood, and Ö. L. Gülder, *Combust. Flame* **136**, 180 (2004).